BioOne DIGITAL LIBRARY

Assessing NASA-POWER Precipitation Product in Predicting Surface Flow: Lower Jhelum River Case Study

Authors: Khalid, Muhammad Raza, Ahmed, Shehroz, and Abdullah, Abdullah

Assessing NASA-POWER Precipitation Product in Predicting Surface Flow: Lower Jhelum River Case Study

Muhammad Raza Khalid[1], Shehroz Ahmed[1] and Abdullah Abdullah[2] (iD)

[1]University of Management and Technology, Lahore, Punjab, Pakistan. [2]University of Campania "Luigi Vanvitell," Aversa, Italy.

ABSTRACT: The Lower Jhelum River watershed has variable topography (i.e. northern mountains and southern plains) and a subtropical climate with hot summers and cool winters. This emphasized the extensive use of state-of-the-art POWER reanalysis precipitation product rather than gauge estimates for hydrological investigations (modeling rainfall runoff, floods, and droughts etc.). To understand the consistency and potential of the precipitation values from both sources, the primary objective of this study was to establish a relationship between POWER data and rain gauge data by utilizing 13 rain gauge stations present in the catchment. While analyzing the rainfall data, a relatively weaker linear association (R), ranging from .6, .68 to .78, was found between the ground-based observatories and the POWER product especially for the arid and semi-arid regions. For the mountainous part, covering a wide glacial range, POWER product showed a better match with ground-based observatories that is, R value ranging from .78, .88 to .91. The simulated stream flow results by integrated HEC-HMS model showed that the POWER product can become a good asset in developing the weather data for those areas where the rain gauges are either absent or inaccessible.

KEYWORDS: POWER product, bias adjustment, stream flows, HEC-HMS, Lower Jhelum Basin

Introduction

Accurate and reliable prediction and assessment of precipitation are valuable for managing water resources, predicting floods and droughts, and meeting agricultural water requirements (Motohashi & Motohashi, 2015; Tapiador et al., 2012). Both observational data and climate model simulations demonstrate complex variations in the amount of rainfall over space and time (Chung et al., 2014; Eyring et al., 2019). The use of a rain gauge has traditionally been a reliable and precise method of monitoring precipitation (Ali et al., 2017); nevertheless, the density of rain gauges is somewhat low in distant areas and near ocean bodies, limiting the uses of rain gauge data for scientific purposes. Weather radar can measure precipitation, but only if the radar systems are widely spaced and calibrated for the kind of precipitation. Since radar requires expensive and complex maintenance, especially in hilly terrains, with limited coverage and shading concerns (De Coning, 2013). In areas with little radar coverage and few rain gauges, remote sensing techniques provide the best alternative for measuring precipitation (De Coning & Poolman, 2011). Globally, numerous gridded precipitation datasets have been created with satellite data (Satgé et al., 2017). Several remotely sensed precipitation products have been developed, including Precipitation Estimation from Remotely Sensed Information using Artificial Neural Network (PERSIANN) (Ashouri et al., 2015), the Multi-Source Weighted-Ensemble Precipitation (MSWEP) (Beck et al., 2017), the Climate Hazard group Infrared Precipitation (CHIRPS) (Funk et al., 2015), and Global Precipitation Measurements from Integrated Multi-satellite Retrievals (GPM-IMERG), which was introduced in 2014 as a follow-up project of Tropical Rainfall Measuring Mission (TRMM) (Huffman et al., 2019).

Various efforts have been made to validate and compare these remotely sensed precipitation products on a regional scale. The GPM-IMERG V5 and V6 were validated throughout Iran by Hosseini-Moghari and Tang (2020) using rain gauge readings, and it was discovered that V5 outperformed V6. Yu et al. assessed the spatial-temporal accuracy of CHIRPS and GPM-IMERG by integrating rain-gauge data with satellite precipitation products, specifically Artificial Neural Networks-Cloud Classification System. Their findings favored the performance of GPM-IMERG over CHIRPS. Meanwhile, Jiang et al. (2021) demonstrated the potential use of IMERG final run precipitation product for monitoring drought conditions in mainland China as an alternative data source. Based on these insights, Arshad et al. (2021) suggested in a separate study that IMERG final run could help bridge the gap in rain-gauge data for weather and flood forecasting purposes. Another way to obtain precipitation data is through reanalysis products, which involve using satellite precipitation retrievals and rain gauges. In addition to this, global atmospheric and land surface reanalysis products are also available. Researchers such as Hu et al. (2016) and Kalnay et al. (1996) have emphasized the significance of these reanalysis products in creating a comprehensive global dataset by integrating satellite and rain gauge precipitation retrievals into model analysis techniques.

Chen et al. (2019) stated that, out of NCEP-2, CFSR, ERA-Interim, JRA-55, and MERRA-2 reanalysis datasets, Modern Era Retrospective Analysis for Research and Applications is considered the most suitable model to portray historical drought patterns across China. Shah and Mishra (2014) assessed reanalysis data from MERRA, ERA-Interim, and CFSR in relation with seasonal monsoon droughts in India. The findings of the study in India revealed a notable positive bias in monsoon season precipitation across the research area for all Reanalysis Precipitation Products.

NASA's Earth Science research program has historically backed satellite systems and investigations that offer essential data for researching climate and climatic events. These datasets contain extended-term climate-averaged assessments of meteorological quantities as well as surface solar energy fluxes. Additionally, time series formatted displays depict the average daily values for fundamental meteorological and solar information. These products derived from satellites and models have demonstrated sufficient accuracy to supply dependable solar and meteorological resource data in areas with limited or no surface measurements. They present two notable benefits: international data coverage and frequent continuity over time.

An extension of the SSE project started in 2003, the Prediction of Worldwide Energy Resources (POWER) project uses weather and sun data from NASA studies to improve building energy efficiency, renewable energy, and agricultural demands. The Modern Era Retrospective-Analysis for Research and Applications assimilation model products from Goddard's Global Modeling and Assimilation Office, along with the GMAO Forward Processing—Instrument Teams and GEOS 5.12.4 near-real-time products, provided the meteorological parameters used in POWER Release 8. The assimilation models differ very little from one another since MERRA-2 and GEOS 5.12.4 are comparable. (Prediction of Worldwide Energy Resources, 2022).

De Aguiar and Lobo (2020) conducted a comparison between weather data obtained from ground stations in Brazil and climatic data sourced from the NASA-POWER database. Their findings revealed a strong correlation between values derived from ground measurements and remotely sensed rainfall, with coefficients ranging from .75 to .95 for most locations. In a separate study, Marzouk (2021) analyzed NASA temperature and precipitation data spanning from 1981 to 2019, concluding that while the air temperature provided by NASA-POWER during 2011 to 2016 was highly reliable, the accuracy of heavy precipitation data was less consistent.

In Pakistan, there has been no previous research analyzing the effectiveness of NASA-POWER for a catchment having variable climate. Therefore, in this study we tried to assess POWER product over Lower Jhelum River Basin. The key objective was to assess how well the POWER records precipitation on monthly time scale. The bias correction and the stream flow result from HEC-HMS model helped us to further evaluate how the product performed before and after the implementation bias correction both on a temporal and spatial scale.

Methodology

Study area

The studied area is Lower Jhelum catchment in which Jhelum River passes through the Jhelum district. It is the largest river of Punjab province. The Jhelum River originates from a spring at Verinag located near the foot of the Pir Panjal in the southeastern part of the Kashmir valley. It flows through Srinagar and Woolar Lake before entering Pakistan through a deep gorge in Kashmir. It is joined by the Kichenganga Neelum, the largest tributary of the Jhelum River, near Muzaffarabad, like Kunhar River in Kagan Valley. The starting point of Lower Jhelum River is taken at the confluence point of both these rivers. The catchment under study extends between 31°00′N–34°30′N latitude and 71°30′E–74°30′E longitude. The position of the Lower Jhelum River Basin in Pakistan, along with the surrounding natural elements have shaped its varied topography and weather patterns. The plain areas possess a humid subtropical climate and is extreme in nature with an average temperature of 49.2°C in summers and 2.7°C in winters. Whereas the mountainous areas like Muzaffarabad and Garhi Dupatta have an average of 27°C in summers and extreme cold with a temperature of –0.6°C. Figure 1 shows the catchment with river tributaries and distribution of rain gauges over the catchment.

Gauge and satellite precipitation data

Monthly precipitation data covering the period from 2014 to 2019 for thirteen (13) gauge stations over Lower Jhelum River catchment was used as a reference in this study, which was obtained from Pakistan Meteorological Department (PMD). The names and location of each gauge station is listed in Table 1.

The Prediction of Worldwide Energy Resource (POWER) Project monthly data was obtained from the National Aeronautics and Space Administration (NASA) Langley Research Center (LaRC) (https://power.larc.nasa.gov/data-access-viewer/). The POWER rainfall database is provided by the Global Precipitation Climate Project (GPCP, version 2.1), which is available at the system's spatial resolution. Other sources, such as microwave imaging, monthly estimates, and atmospheric infrared sounders, are also consulted to compile more accurate estimates (Stackhouse et al., 2016). NASA-POWER makes use of gridded datasets that collect precipitation data from many sources. It estimates precipitation values between grid cells using interpolation approaches, leading to the extraction of point-specific rainfall data. Spatial resampling removes or interpolates precipitation quantities at specific places, making point rainfall data more accessible. Users may obtain point precipitation data by giving latitude and longitude coordinates or choosing areas using the POWER platform's
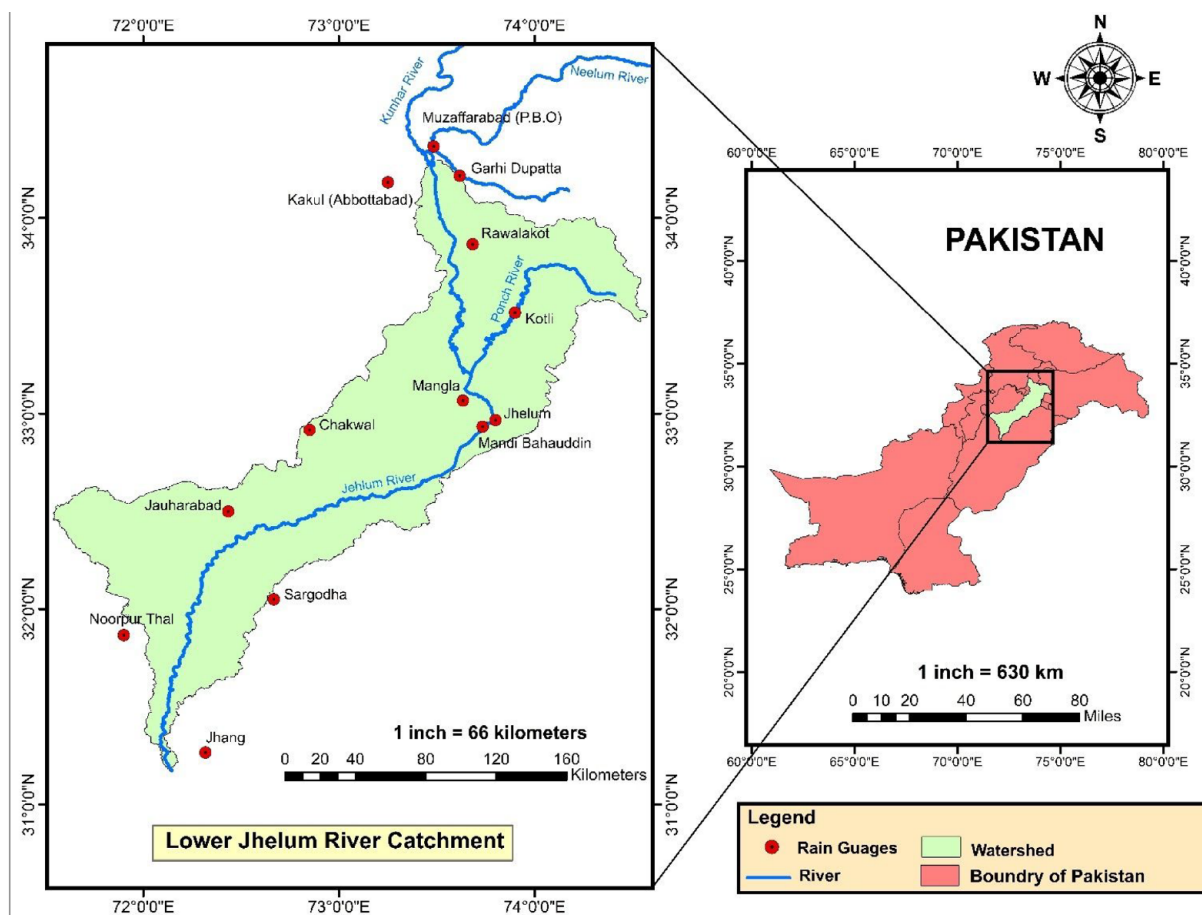
Figure 1. Study area with river tributaries and locations of rain gauge stations.

Table 1. Specifics of Rain Gauge Stations.

ID	STATIONS	LATITUDE (Y)	LONGITUDE (X)	ELEVATION (M)
1	Kakul	34°11′	72° 15′	1,308
2	Garhi Dupatta	34°13′	73°37′	813.5
3	Muzaffarabad	34°22′	73°29′	702
4	Rawalakot	33°52′	73°41′	1,677
5	Kotli	33°31′	73°54′	614
6	Mangla	33°4′	73°38′	283.3
7	Jhelum	32°56′	73°44′	287.19
8	Mandi Bahauddin	32°58′	73°48′	252.97
9	Chakwal	32°55′	72°51′	519
10	Jauharabad	33°30′	72°26′	187
11	Sargodha	32°3′	72°40′	187
12	Noorpur Thal	31°52′	71°54′	186
13	Jhang	31°16′	72°19′	158

Table 2. Specifications of POWER Dataset.

Spatial resolution	0.5° (55.5 km) latitude by 0.5° (55.5 km) longitude
Reference satellite	GPCP
Sensor	Infrared and microwave
Temporal coverage	1 January 1997 to near present

map interface. The monthly data was downloaded by inserting the coordinates of the gauge stations. The specifications of the POWER dataset are given in Table 2.

Digital elevation model

The topography was described using a DEM, which identifies every point's elevation inside a given area at a specific spatial resolution. A 30 m by 30 m resolution DEM was acquired from the SRTM (Shuttle Radar Topography Mission) website (https://earthexplorer.usgs.gov/).

With the help of reference elevation points provided by PMD, the DEM was analyzed. The discrepancies between the values of each DEM pixel and the existing elevations were used for the validation of DEM. When the elevation error was estimated, positive differences indicated that the DEM elevation

was higher than the actual point elevation. Similarly, the negative errors occurred when the DEM elevation was lower than the actual elevation. Our analysis showed negative errors for most of the analyzed pixel cells, indicating that the elevation of the DEM was lower than the elevation of the actual.

$$\text{Elevation Error } Z_{diff} = Z_{DEM} - Z_{PMD}$$

Thiessen polygons for average basin rainfall

The reliable modeling of flash flood values can only be achieved if the factual average rainfall estimates for the basin are available. The average basin rainfall represents a single rainfall value for a specific period, but uniformly distributed over the entire watershed. To incorporate the response of entire catchment, the availability of reliable average basin rainfall is essential. By increasing the number of rain gauge stations, the obtained values of average basin rainfall become more reliable and significant for hydrological investigations in the catchment. Therefore, average basin rainfall was obtained by means of the Thiessen Polygon Algorithm in ArcGIS (Saber & Yilmaz, 2018). The resulting Thiessen weights were then multiplied with the precipitation of each rain gauge station to obtain the average basin rainfall. Figure 2 shows the Thiessen polygons and the corresponding weights for each station.
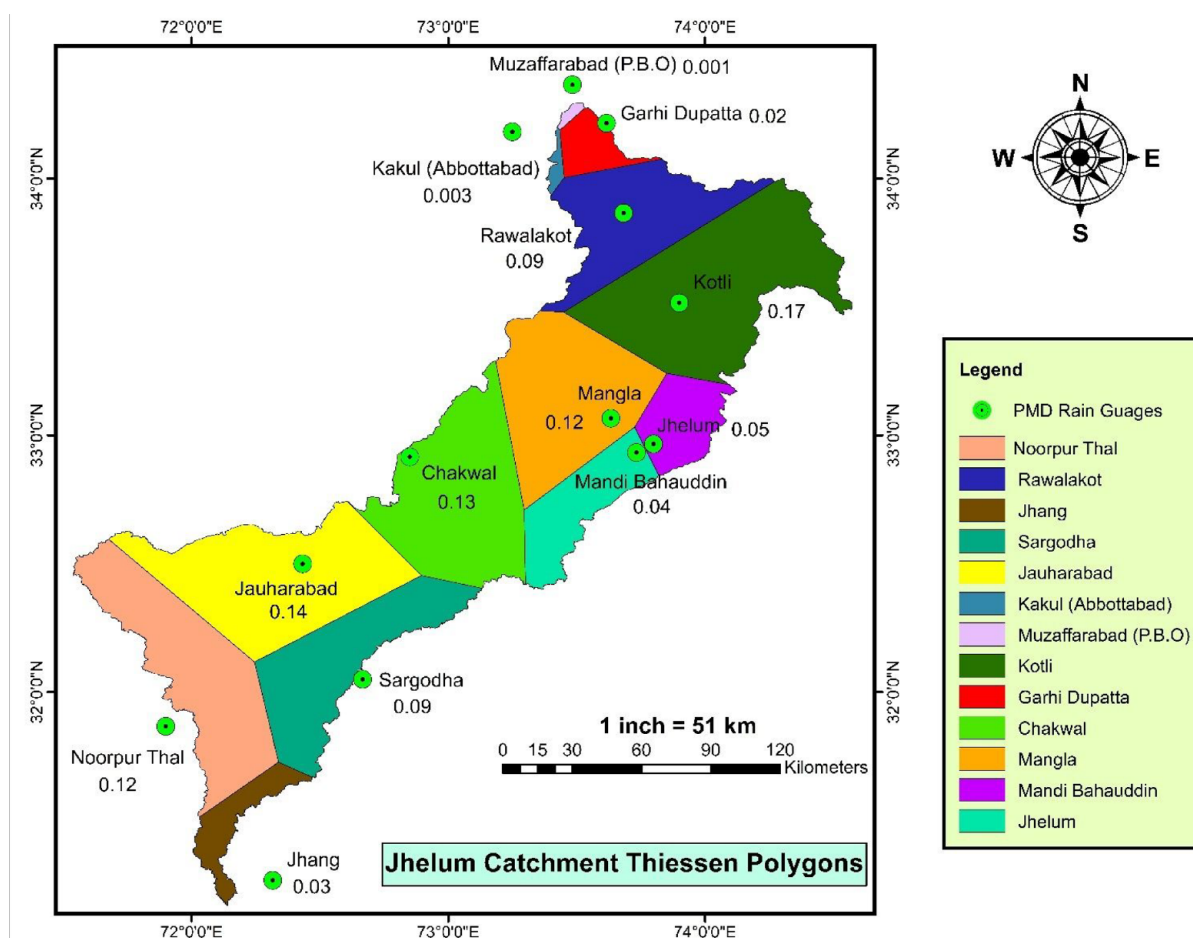
Figure 2. Thiessen polygons and weights for each station.

Table 3. Description of the Statistical and Performance Parameters.

INDEX	FORMULAS	UNIT	BEST VALUES
Bias error (*BE*)	$$BE = \frac{1}{n}\sum_{i=1}^{n}\left(S_i - G\right)$$	mm	0
Relative bias (*RE*)	$$RB = \frac{\sum_{i=1}^{n}\left(S_i - G\right)}{\sum_{i=1}^{n}G} \times 100$$	%	0
Root mean square error (RMSE)	$$RMSE = \sqrt{\frac{1}{n}\sum_{i=1}^{n}\left(S_i - G\right)^2}$$	mm	0
Correlation coefficient (*R*)	$$CC = \frac{\sum_{i=1}^{n}\left(G_i - \overline{G}\right)\left(S_i - \overline{S}\right)}{\sqrt{\sum_{i=1}^{n}\left(G_i - \overline{G}\right)^2}\sqrt{\sum_{i=1}^{n}\left(S_i - \overline{S}\right)^2}}$$	NA	1
False alarm ratio (FAR)	$$FAR = \frac{False\ Alarms}{Hits\ +\ False\ Alarms}$$	NA	0
Probability of detection (POD)	$$POD = \frac{Hits}{Hits\ +\ Misses}$$	NA	1
Critical success index (CSI)	$$CSI = \frac{Hits}{Hits\ +\ False\ Alarms\ +\ Misses}$$	NA	1

Bias correction

To carry out hydrological investigation the rain estimates provided by the SPPs must be as precise as possible. Therefore, multiplicative bias factor technique was employed to adjust the satellite estimates (Saber & Yilmaz, 2018). The bias factor is a scaling factor that is used to adjust the bias in the estimated outcome measure. Due to insufficient historical data from rain gauge stations, this technique is used. The equation for bias factor is given as:

$$Bias\ Factor = \frac{Gauge\ Precipitation}{Model\ Precipitation}$$

$$M_{i\_corr} = BF \times M_i$$

Initially, the bias factor for each month was determined using the bias factor formula. The bias factor values were then averaged across two consecutive months to provide a single value. This single value was multiplied by the uncorrected values of the satellite estimates of 2 months. This technique was applied for the next 2 months as well.

Tatistical and performance parameters

To evaluate the performance of POWER product, it was compared with the observed rain gauge product before and after the implementation of bias correction respectively. For this purpose, three performance parameters were evaluated including False Alarm Ratio (FAR) which is the ratio of no. of rain events falsely reported to total number of reported events, Probability of Detection (POD) which the ratio of no. of rain events accurately reported to total number of events (accurately reported plus missed) and Critical Success Index (CSI) which is the ratio of no. of rain events accurately reported to total number of events (accurately reported plus missed plus falsely reported). Moreover, four statistical parameters were also used that is, Relative Bias (*RE*) which gives the percentage error present in a dataset, the Mean Error or Bias Error (*ME/BE*) which gives simple error, the Correlation Coefficient (*R*) which tells us about the linear association between two datasets and the Root Mean Square Error (RMSE) which is highly sensitive to the value of error that is, if there is bigger error in data RMSE value would be higher and vice versa (Le et al., 2018). Table 3 provides the description about these parameters.
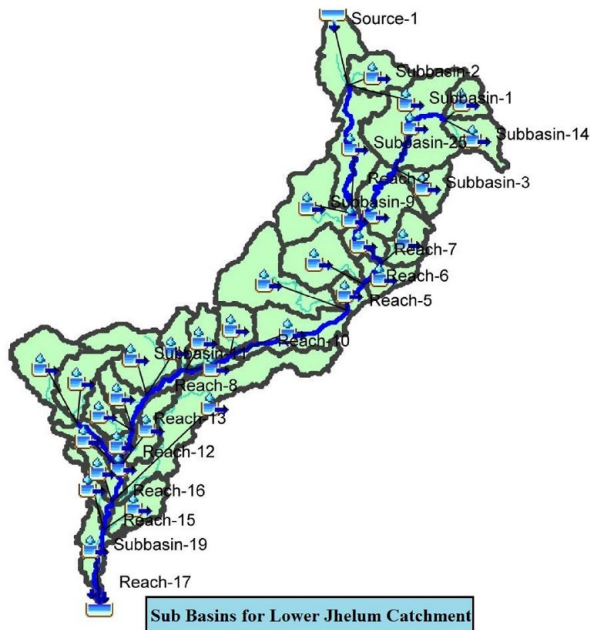
Figure 3. Lower Jhelum River Basin with sub-basins distributions in HEC-HMS.

Table 4. Description of NRSC Soil Groups (James et. al., 2010).

GROUP	DESCRIPTION	SATURATED HYDRAULIC CONDUCTIVITY (IN/HR)
A	High infiltration rates, well to excessively drained sands or gravels.	⩾0.45
B	Moderate infiltration rates, shallow loses, sandy loam.	0.30−0.15
C	Slow infiltration rates, clay loams, shallow sandy loam.	0.15−0.05
D	Very slow infiltration rates, consisting chiefly of clay soil.	0.05−0

Table 5. Curve Numbers for Hydrologic Soil Groups. Technical Release 55 (USDA-NRCS, 1986).

LAND COVER TYPE	CURVE NUMBER			
	A	B	C	D
Water	98	98	98	98
Forest	30	55	70	77
Wetlands	87	89	90	91
Agriculture	70	80	83	90
Urban	80	88	91	93
Barren land	77	86	91	94

where, n is the total number of gauge stations; S_i is the satellite-built estimates and G is the observed rainfall value by the gauge. The "*Hits*" are the events which are correctly measured by both the gauge and the POWER product. "*False Alarms*" represents the false values predicted by the POWER product when there was no rainfall in actual. "*Misses*" represents the values which were missed by the POWER product when there was a rainfall in real.

Hydrological modeling

The HEC-HMS watershed model was utilized to analyze the impact of topography, land use, soil, and weather conditions on stream flow in the Lower Jhelum River Basin from 2014 to 2019. The hydrological modeling in HEC-HMS involved using the SCS-Curve Number method for loss estimation, SCS-Unit Hydrograph method for runoff estimation, and Muskingum method for flow routing. The study sought to assess changes in stream flow following bias correction.

The basin was initially defined by delineating 19 sub-basins, which were based on the physical characteristics of the study area, including land use and land cover, soil distribution as well as topographical features. This process was carried out using ArcGIS tools and analysis. The sub-basins are shown in the Figure 3. The determination of a curve number necessitates understanding the hydrologic soil group, which signifies the degree of infiltration for different soil types. There exist four classifications of hydrologic soil groups: A, B, C, and D. These groupings and their definitions are listed in Table 4. The Curve Number table developed by the Soil Conservation Service

presents CN values for various land use and hydrologic soil group combinations. The CN is a unit less parameter that varies from 0 (indicating high infiltration) to 100 (indicating no infiltration). The CN map was created by combining hydrologic soil groups and land use configurations. Table 5 shows the CN values adopted from Technical Release 55 (USDA-NRCS, 1986). In order to compute rainfall runoff, the SCS-CN loss approach has been utilized. The CN approach for evaluating infiltration requires an estimate of the CN for each sub-basin. The SCS-UH approach (Barman & Bhattacharjya, 2020; Khaddor et al., 2017; Tassew et al., 2019) was used to calculate outflow at a certain outlet, needing lag time and percentage impervious area of it. A hydrograph of the upstream boundary conditions was provided at Kohala Station, and the basin's lag time was set at 0.6 times the concentration time. The Muskingum method is one of the various techniques used by HEC-HMS to calculate stream flow at the basin's outlet. It is an easy approach that doesn't require multiple inputs, as noted by Song et al. (2011) and Tassew et al. (2019).

The system of equations for Lag time (L), Time of concentration (T_c), and maximum retention time (S) in HEC-HMS are illustrated below.
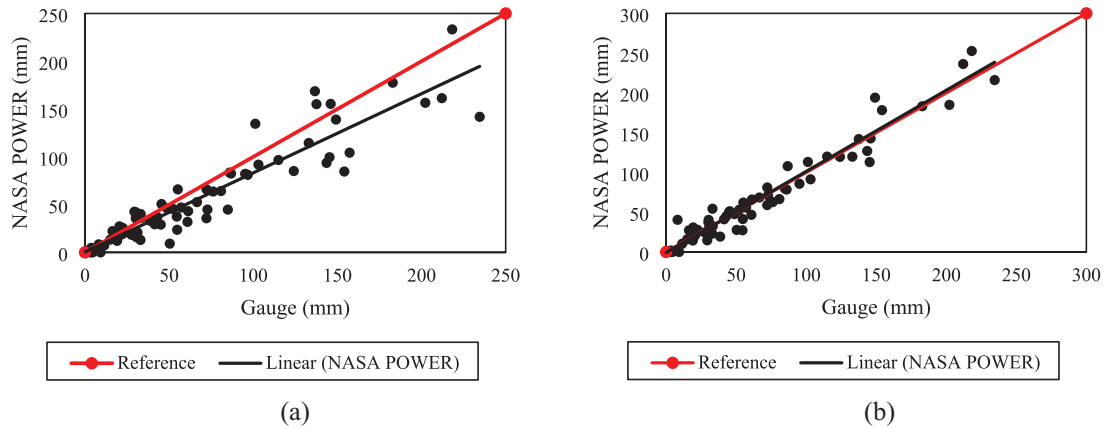
Figure 4. (a) Monthly average basin rainfall before correction. (b) Monthly average basin rainfall after correction.

$$S = \frac{1000}{\text{CN}} - 10$$

$$L = 0.6T_c$$

$$T_c = \frac{\ell^{0.8}(S+1)^{0.7}}{1140Y^{0.5}}$$

Where S is maximum soil retention (mm) and CN is the Curve Number, T_c is time of concentration (hours), ℓ is flow length (ft), Y is average watershed land slope (%) and S is maximum soil retention (in).

Results

Comparison of average basin rainfall

Before the application of the multiplicative bias removal factor for average basin rainfall, the two datasets were demonstrating the B value of –11.32, which showed underestimation, that is, the product underestimated the rainfall as compared to gauge, *RE* value of –16.53%, which was also a sign of underestimation by the POWER product. The gauge and satellite datasets were found to be connected in a strong way, as indicated by R being .93. However, the POD was 0.62, which is good but not decent, and the FAR was 0.78, which showed that there were numerous events when POWER predicted some rainfall value but originally there wasn't any precipitation. Around 20% of POWER's data was found to be accurately captured. After using the bias correction factor, the parameters revealed positive results. *BE*'s value after rectification was 0.63, demonstrating convergence to the optimum value of zero. Likewise, the result of *RE* –0.92% indicated convergence to the standard value. The value of R was increased to .96, which demonstrated an enhanced relationship between gauge and POWER product. The behavior for bias correction for average basin rainfall is illustrated in Figure 4a and b scatter plots.

Comparison of point precipitation of entire study area

For whole study area the point data for all the stations was gathered to plot the scatter plot and to evaluate the parameters. Thorough comparison between ground-based rain estimates and NASA-POWER product for point-based rainfall was achieved, initially by making the comparison for point rainfall, for each rain station and then for all stations covering the study area. The statistical indices were expansively estimated and examined, earlier and later the implementation of bias adjustment procedure on NASA-POWER monthly estimates. The examined statistical indicators were *RE*, *R*, RMSE, and *BE* respectively. The performance evaluating indices for the categorial based validation were analyzed just for NASA-POWER product that is, they were not assessed after the implementation of bias amendment, as the assessment of performance of the NASA-POWER sensor was required. The indices evaluating both the estimation and performance of NASA-POWER are presented in Table 6 and 7. It was observed that heavy rain events ($>$10 mm) were usually underestimated by NASA-POWER, while lighter rain events were mainly overestimated by it. Prior to the application of the multiplicative bias removal factor, the two datasets exhibited a *BE* value of –0.05, indicating underestimation, that is, the model underestimated the precipitation compared to the gauge (*RE* value being –0.03%), which was also an underestimated signal. The RMSE score of 0.70 revealed convergence of data to the reference line. The correlation coefficient reached to .82, indicating a very strong relationship between the gauge and satellite dataset. However, the POD was 0.21, which is good but not ideal, and the FAR was 0.18, indicating that there were less occasions for which the product predicted precipitation but there was no precipitation. CSI value was determined to be 0.2, meaning that only 0.2 out of 1 part of data was accurately evaluated. Applying the bias correction factor directed us to quite appreciable

Table 6. Statistical Parameters for Multiple Scenarios Before Bias Correction.

STATIONS	*BE/ME*	*RE/PB* (%)	RMSE	*R*	POD	FAR	CSI
Chakwal	1.31	2.14	36.85	.82	0.22	0.12	0.22
Garhi Dupatta	−29.39	−27.31	51.25	.86	0.13	0.1	0.13
Jauharabad	−5.07	−11.26	43.48	.6	0.13	0.38	0.12
Jhang	−6.99	−19.87	48.29	.68	0.12	0.5	0.1
Jhelum	0.87	1.24	38.93	.89	0.15	0.23	0.14
Kakul	−26.47	−24.88	43.09	.91	0.09	0.14	0.08
Kotli	−21.12	−21.05	61.42	.8	0.12	0.11	0.12
Mandi Bahauddin	1.68	2.42	43.08	.85	0.2	0.25	0.17
Mangla	−8.01	−10.12	46.92	.81	0.12	0.11	0.12
Muzaffarabad	−38.58	−34	59.39	.88	0.13	0	0.13
Noorpur Thal	−4.45	−13.95	38.94	.66	0.09	0.4	0.09
Rawalakot	−45.34	−36.69	87.48	.78	0.06	0.33	0.06
Sargodha	−11.5	−25.36	30.73	.87	0.09	0.45	0.09
Average basin rainfall	−11.32	−16.53	24.12	.93	0.21	0.18	0.2
Entire study area	−0.05	−0.03	0.70	.82	0.21	0.18	0.2

Table 7. Statistical Parameters for Multiple Scenarios After Bias Correction.

STATIONS	*BE/ME*	*RE/PB* (%)	RMSE	*R*
Chakwal	0.23	0.37	25.23	.9
Garhi Dupatta	1.21	1.13	33.10	.91
Jauharabad	2.18	6.24	38.93	.7
Jhang	0.28	0.9	35.21	.66
Jhelum	0.61	0.87	26.77	.95
Kakul	1.4	1.3	30.52	.94
Kotli	−3.16	−3.15	47.91	.87
Mandi Bahauddin	0.09	0.13	31.80	.93
Mangla	0.37	0.47	24.01	.95
Muzaffarabad	0.7	0.6	29.39	.93
Noorpur Thal	4.4	13.93	31.97	.76
Rawalakot	−1.54	−1.24	42.28	.93
Sargodha	1.61	3.55	29.2	.9
Average basin rainfall	0.63	0.92	16.98	.96
Study area	0.06	0.01	0.29	.9

parameters for the study area. After being adjusted, the values for *BE*, *RE*, RMSE, and *R* were 0.06, 0.01%, 0.29, and .9. Convergence to the reference value is found in all the parameters. There was an increase in the *R* value, suggesting a higher relationship between the gauge and the product. Figure 5a and b demonstrate the behavior of data for the entire
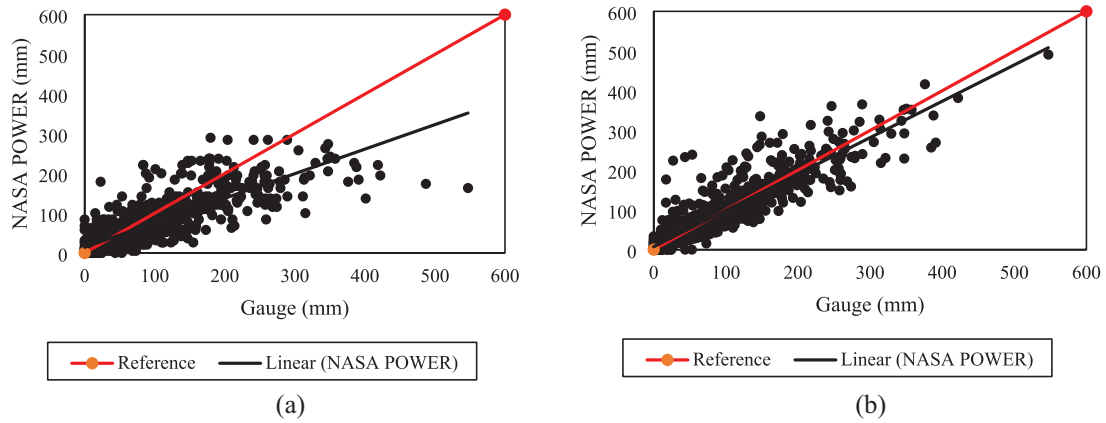
Figure 5. (a) Monthly point rainfall of entire study area before correction. (b) Monthly point rainfall of entire study area after correction.
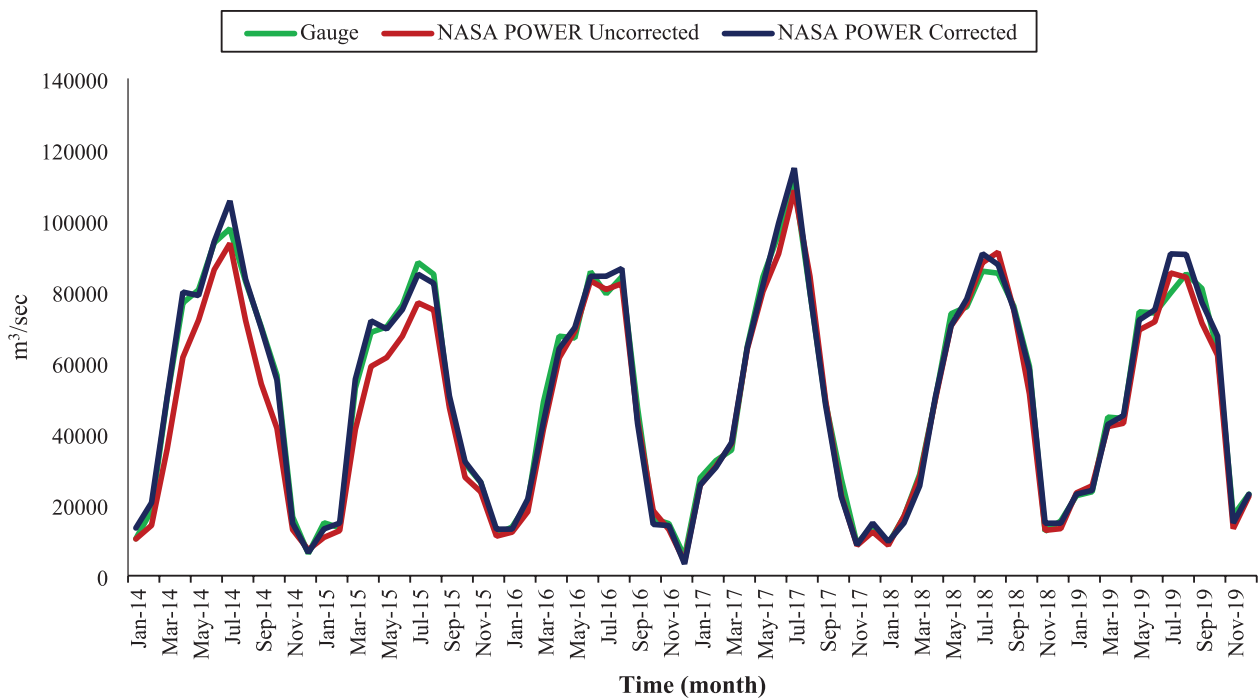
Figure 6. Stream flows generated in HEC-HMS by utilizing average basin rainfall of gauges, uncorrected and corrected POWER datasets.

study area by means of a linear scatter plot. The results for all station before and after the bias correction are shown in Tables 6 and 7 in tabular form.

Estimation of outflows for lower Jhelum River Basin

For evaluating the generated stream flows, a comparison of average basin rainfall of gauge, uncorrected and corrected POWER product was made. In case of average basin rainfall for gauge, the peak flow was observed in July 2017 with a value of 1,10,804 m^3/s. When comparing it with the average basin rainfall for uncorrected POWER product, the peak flow was observed as 1,08,484.7 m^3/s in the month of July 2017.

Although the peak flows observed in both the cases were in the month of July 2017 but difference in the values can be seen evidently. The model results improved when amended average basin rainfall was utilized. Likewise, the peak flow was seen in July 2017 with a value of 1,14,750.3 m^3/s. When comparing this value with the other two datasets, the results were improved but there was some overestimation in the outflows. Figure 6 is depicting the outflows for gauge, uncorrected and corrected POWER based average basin rainfall. Statistical parameters such as *BE*, *RE*, RMSE, and *R* were also determined to evaluate the amount of error before the correction. The parameters *BE*, *RE*, RMSE, and *R* showed a value of 329, 6.96%, 5,809 and .98 respectively. The three parameters other than *R* showed the huge error but after the implementation of bias correction
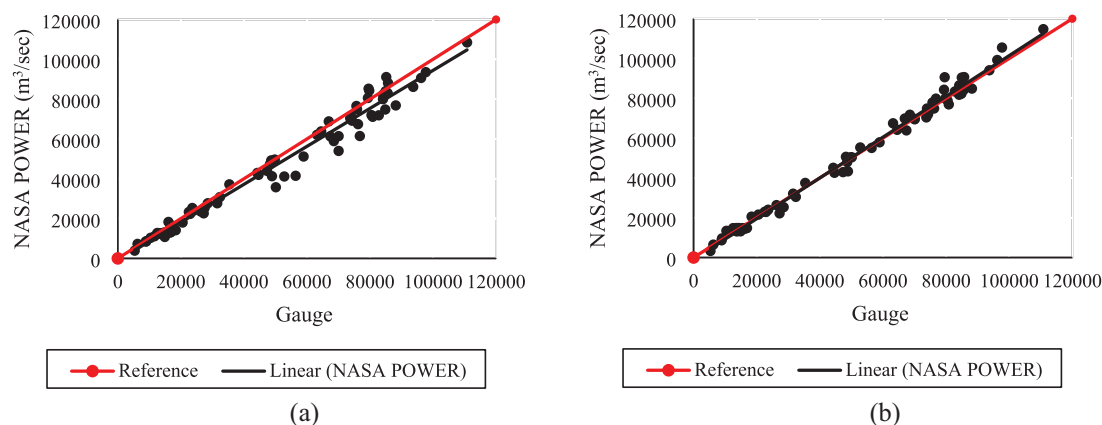
Figure 7. (a) Stream flow comparison before correction. (b) Stream flow comparison after correction.
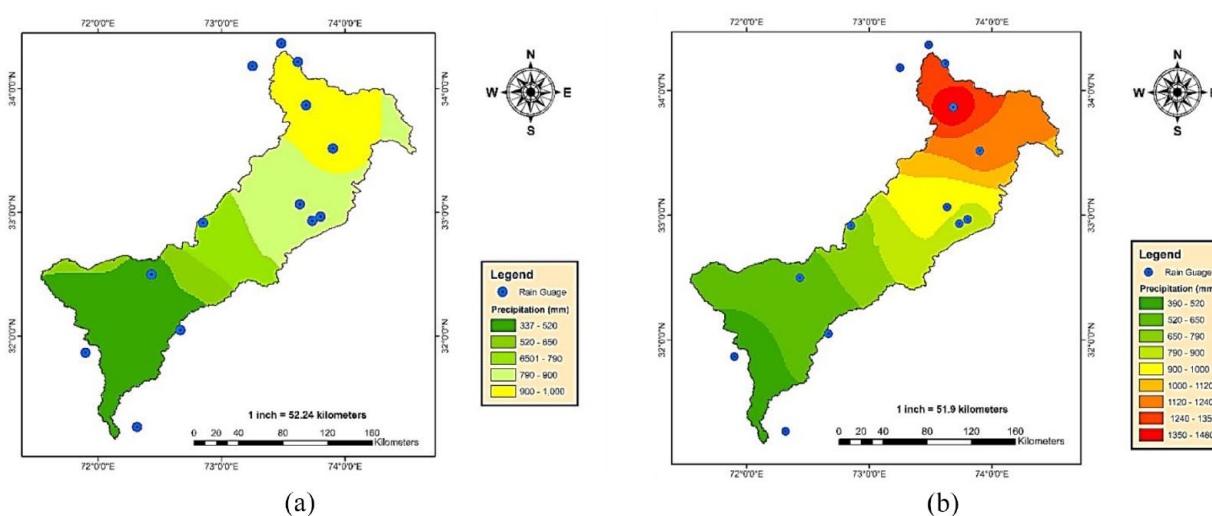
Figure 8. (a) Mean annual rainfall of POWER dataset before bias correction. (b). Mean annual rainfall of gauge dataset.

the improvement in the results can be seen. Likewise, to visualize the effect of bias correction linear scatter plots are shown in Figure 7a and b for visualizing the behavioral impact of data on runoff simulations. It can be said on this base that smaller value of mean error in rainfall estimates leads to bigger values of mean errors in results of hydrological investigations. Therefore, use of reliable global rainfall estimates for hydrologic use must be made. There exist many possibilities for the occurrence of inaccuracies in results of model that is, the bias adjustment procedure or the chances of error in gauge-based estimates due to influence of wind, interception losses, splash, and evaporation effects (Saber & Yilmaz, 2018).

Since, the hydrological modeling was performed to see the peak flows and their time for peak, so the model calibration was accomplished to adjust the driving parameters of model in such a way that both hydrographs that is, observed and simulated came closer to each other in all cases. With the help of auto optimization manager in HEC-HMS, the calibration of model was conducted for rainy months that is, July to September. The model's sensitivity was improved by applying auto optimization repeatedly. The performance of model

during these calibration trials was assessed through statistical indices *BE*, RMSE, *RE*, and *R* correspondingly. As far as validation of model is concerned, it was achieved by considering a smaller hypothetical catchment, but the months for validation were changed that is, from April to June were selected for 11 years.

Mean average rain maps

Rain is usually presented as a map to display rainfall spatial and temporal variation over certain periods of time and land areas with a color range. The rainfall maps were developed in ArcGIS by utilizing the gauge, uncorrected and corrected POWER rainfall data. For our study area over a 6-years period, we created mean annual rainfall maps to demonstrate how the Lower Jhelum catchment's rainfall differ in both space and time. It is also evident from the below diagrams that as the terrain become mountainous the behavior of the POWER product becomes complex and biased. Figures 8a and b and 9a and b display the mean average rainfall maps before and after the application of bias correction.
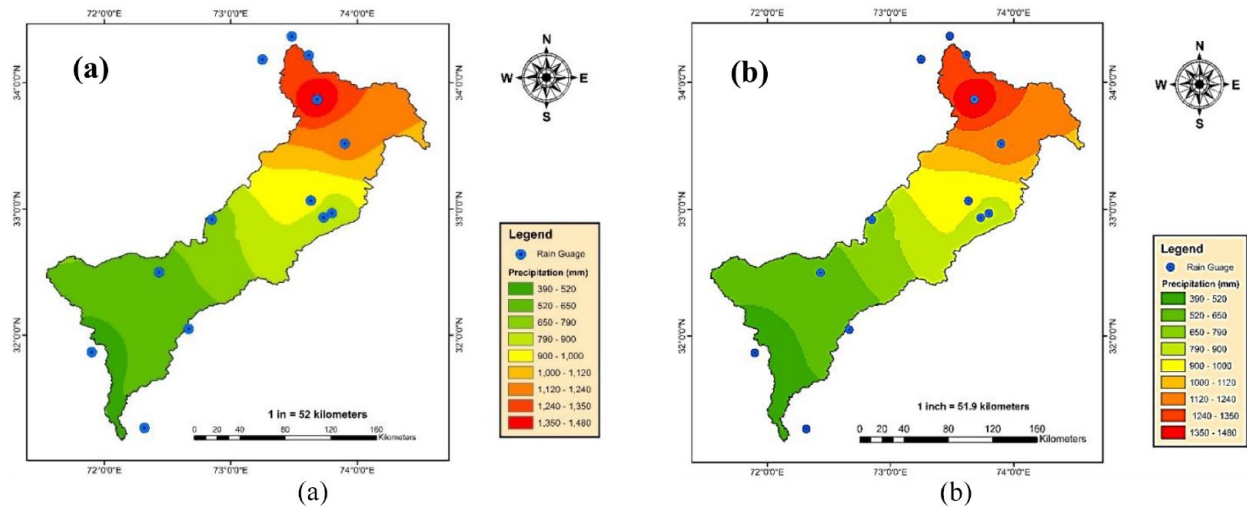
Figure 9. (a) Mean annual rainfall of POWER dataset after bias correction. (b) Mean annual rainfall of gauge dataset.

Discussions of results

The evaluation of NASA-POWER estimates relative to gauge products was made with the help of few statistical indices that is, RMSE, *BE*, *RE*, and coefficient for linear correlation (*R*) (Tables 6 and 7). *BE* shows the mean value of error available in NASA-POWER relative to gauge estimates. Its value can be either positive or negative, representing overestimation and underestimation accordingly. *RE* parameter also indicates overestimates or underestimates of rainfall depending upon the negative or positive value. The absolute measure of mean error is sensed by RMSE and is the most used parameter of statistics. It is found to be sensitive to bigger values of bias (Chu & Shirmohammadi, 2004; Singh, 2005). While the linear association between the two datasets is represented by *R*.

Moreover, for the assessment of sensor of NASA-POWER product, three functionality evaluating indices were also used namely, POD that is, Probability for Detection of rainfall events, FAR that is, False Alarm Ratio and CSI that is, Critical-Success Index. POD represents the rate for hit rain events that is, the proportion of events which are correctly perceived by NASA-POWER, the range is from 0 to 1. FAR shows the fraction of rain events inaccurately captured. While CSI tells us the fraction of successfully read rain events by NASA-POWER. All the above-mentioned statistical indices are given in Table 4 along with their best figures.

Hydro-meteorological research greatly depend on the accurate spatial and temporal estimation of precipitation. When obtaining spatially distributed rainfall estimates at regional and global dimensions, satellite-based products are frequently used (Abdullah et al., 2020). Based on our findings, it was found that NASA-POWER in this instance significantly underestimates rainfall when compared to rain gauges. Orographic effects, which induce moist air to rise over mountains and generate rain shadows on leeward slopes and increased rainfall on windward slopes, are common in variable topographical regions.

Underestimating the amount of rainfall across a basin may take place when rainfall estimation models fail to appropriately account for these orographic effects (Sun et al., 2020). This behavior was clearly observed in mean annual rain maps. Short-duration, intense rainfall events that considerably increase the total amount of precipitation throughout a basin might not have been captured by the temporal resolution of NASA-POWER data. Underestimating average basin rainfall over a given time may arise by failing to record these heavy rainfall events. Localized characteristics that may not be adequately captured in the dataset can be found on plains, such as lakes, tiny hills, rivers, and variations in land cover and use. Errors in point rainfall estimates may result from missing these features (Shah & Mishra, 2014).

The quality and availability of field-based observations that are utilized to test and calibrate the models have a significant impact on the accuracy of rainfall estimates. The dataset might be deficient in information needed to appropriately depict regional rainfall patterns in places with a low density of ground-based meteorological stations which could be another reason for the underestimation of rainfall (Yu et al., 2020).

Limitations

Although NASA-POWER product provides useful information about climatological and meteorological factors, such as precipitation, it possesses several limitations, most notably regarding bias correction. Particularly in areas with few or weak observational networks, bias correction approaches may be sensitive to the quantity and quality of reference data used for calibration, which could result in errors. The research was conducted using the monthly precipitation data for 6 years.

Conclusion

The results of study showed that POWER tends to underestimate the rainy events in mountainous region like Muzaffarabad,

Garhi Dupatta, Kakul. The reason for the uncertainty between the gauge and satellite-based estimates is probably the proximity of mountains in these regions. The mountains' steep topography expedites the abrupt and rapid growth of rain clouds, resulting in successive sensor snapshots of miss events.

However, for the plain areas it shows overestimation for Jhelum, Mandi Bahuddin and Chakwal stations. While for Jhang, Sargodha, Jauharabad, and Noorpur Thal it shows underestimation. The possible reason for this can be the complexity of the topography and the dry seasons present in these areas. Due to which there is a possibility of satellite to detect the lower or greater thresholds of precipitation.

After incorporating the bias factor, the satellite's ability to reproduce precipitation patterns increased adequately. The parameters like *R*, *BE*, and *RE* showed good results after the implementation of bias factor. However, RMSE being very sensitive to bias values illustrates that the error between the gauge and satellite-based estimates was due to error in bigger rain events. The categorial authentication parameters that is, POD, FAR and CSI discovered that the rainfall data from POWER product has a far better quality than many other SPPs. This can be due to better agreement of rainfall governing factors (on which POWER product is based) with the climate and topography of our region. The results of hydrological modeling revealed that the POWER product can become a good asset in developing the weather data for those areas where the rain gauges are either absent or inaccessible.

Future Scope

To improve bias correction models, especially in regions with few ground-based data or intricate topography features, the future scope of the research will involve investigating machine learning algorithms and modern-day statistical techniques. Moreover, the utilization of high-resolution satellite data could provide more accurate bias correction, thereby increasing the usefulness of NASA-POWER in hydrological modeling, renewable energy assessments, and climate research.

Author Contributions

The authors declare that no funding was received from any source to conduct this research. Moreover, the authors contribution is provided as: Muhammad Raza Khalid: Modeling on HEC-HMS and ArcGIS. Shehroz Ahmed: Bias correction and graphical representation. Abdullah: Drafting and Methodology.

Declaration of Conflicting Interests

The author(s) declared no potential conflicts of interest with respect to the research, authorship, and/or publication of this article.

Funding

The author(s) received no financial support for the research, authorship, and/or publication of this article.

ORCID iD

Abdullah Abdullah [iD] https://orcid.org/0000-0001-8084-3160

REFERENCES

Abdullah, H. U. R., & Mirza, M. A. (2020). Statistical analysis and bias correction of GSMaP satellite rainfall data for flash floods modelling over the Basin of Ravi River. *International Journal on Emerging Technologies*, 11(5), 545–557.

Ali, A., Xiao, C., Anjum, M., Adnan, M., Nawaz, Z., Ijaz, M., Sajid, M., & Farid, H. (2017). Evaluation and comparison of TRMM multi-satellite precipitation products with reference to rain gauge observations in Hunza River Basin, Karakoram range, northern Pakistan. *Sustainability*, 9(11), 1954. https://doi.org/10.3390/su9111954.

Arshad, M., Ma, X., Yin, J., Ullah, W., Ali, G., Ullah, S., Liu, M., Shahzaman, M., & Ullah, I. (2021). Evaluation of GPM-IMERG and TRMM-3B42 precipitation products over Pakistan. *Atmospheric Research*, 249, 105341. https://doi.org/10.1016/j.atmosres.2020.105341.

Ashouri, H., Hsu, K.-L., Sorooshian, S., Braithwaite, D. K., Knapp, K. R., Cecil, L. D., Nelson, B. R., & Prat, O. P. (2015). PERSIANN-CDR: Daily precipitation climate data record from multisatellite observations for hydrological and climate studies. *Bulletin of the American Meteorological Society*, 96(1), 69–83. https://doi.org/10.1175/BAMS-D-13-00068.1.

Barman, S., & Bhattacharjya, R. K. (2020). ANN-SCS-based hybrid model in conjunction with GCM to evaluate the impact of climate change on the flow scenario of the River Subansiri. *Journal of Water and Climate Change*, 11(4), 1–5.

Beck, H. E., van Dijk, A. I. J. M., Levizzani, V., Schellekens, J., Miralles, D. G., Martens, B., & de Roo, A. (2017). MSWEP: 3-hourly 0.25 global gridded precipitation (1979–2015) by merging gauge, satellite, and reanalysis data. *Hydrology and Earth System Sciences*, 21(1), 589–615. https://doi.org/10.5194/hess-21-589-2017.

Chen, S., Gan, T. Y., Tan, X., Shao, D., & Zhu, J. (2019). Assessment of CFSR, ERA-interim, JRA-55, MERRA-2, NCEP-2 reanalysis data for drought analysis over China. *Climate Dynamics*, 53, 737–757. https://doi.org/10.1007/s00382-018-04611-1.

Chu, T. W., & Shirmohammadi, A. (2004). Evaluation of the SWAT model's hydrology component in the piedmont physiographic region of Maryland. *Transactions of the ASAE*, 47(4), 1057.

Chung, C. T. Y., Power, S. B., Arblaster, J. M., Rashid, H. A., & Roff, G. L. (2014). Nonlinear precipitation response to El Ni~no and global warming in the Indo-Pacific. *Climate Dynamics*, 42(7–8), 1837–1856. https://doi.org/10.1007/s00382-013-1892-8.

De Aguiar, J. T., & Lobo, M. Jr. (2020). Reliability and discrepancies of rainfall and temperatures from remote sensing and Brazilian ground weather stations. *Remote Sensing Applications: Society and Environment*, 18, 100301.

De Coning, E. (2013). Optimizing satellite-based precipitation estimation for nowcasting of rainfall and flash flood events over the South African domain. *Remote Sensing*, 5(11), 5702–5724. https://doi.org/10.3390/rs5115702.

De Coning, E., & Poolman, E. (2011). South African Weather Service operational satellite-based precipitation estimation technique: Applications and improvements. *Hydrology and Earth System Sciences*, 15(4), 1131–1145. https://doi.org/10.5194/hess-15-1131-2011.

Eyring, V., Cox, P. M., Flato, G. M., Gleckler, P. J., Abramowitz, G., Caldwell, P., Collins, W. D., Gier, B. K., Hall, A. D., Hoffman, F. M., Hurtt, G. C., Jahn, A., Jones, C. D., Klein, S. A., Krasting, J. P., Kwiatkowski, L., Lorenz, R., Maloney, E., Meehl, G. A., . . . Williamson, M. S. (2019). Taking climate model evaluation to the next level. *Nature Climate Change*, 9, 102–110. https://doi.org/10.1038/s41558-018-0355-y.

Funk, C., Peterson, P., Landsfeld, M., Pedreros, D., Verdin, J., Shukla, S., Husak, G., Rowland, J., Harrison, L., Hoell, A., & Michaelsen, J. (2015). The climate hazards infrared precipitation with stations—a new environmental record for monitoring extremes. *Scientific Data*, 2, 150066. https://doi.org/10.1038/sdata.2015.66.

Hosseini-Moghari, S.-M., & Tang, Q. (2020). Validation of GPM IMERG V05 and V06 precipitation products over Iran. *Journal of Hydrometeorology*, 21, 1011–1037. https://doi.org/10.1175/JHM-D-19-0269.1.

Hu, Z., Hu, Q., Zhang, C., Chen, X., & Li, Q. (2016). Evaluation of reanalysis, spatially interpolated and satellite remotely sensed precipitation data sets in central Asia. *Journal of Geophysical Research: Atmospheres*, 121(10), 5648–5663. https://doi.org/10.1002/2016JD024781.

Huffman, G. J., Bolvin, D. T., Braithwaite, D., Hsu, K. L., Joyce, R., Kidd, C., Nelkin, E. J., Sorooshian, S., Tan, J., & Xie, P. (2019). *NASA global precipitation measurement (GPM) integrated multi-satellitE retrievals for GPM (IMERG)* (Algorithm theoretical basis document (ATBD) version 06). National Aeronautics and Space Administration, 1–34.

James, W. R. C., Rossman, L. E., & James, W. (2010). *User's guide to SWMM5* (12th ed.). Computational Hydraulic International (CHI).

Jiang, S., Wei, L., Ren, L., Xu, C.-Y., Zhong, F., Wang, M., Zhang, L., Yuan, F., & Liu, Y. (2021). Utility of integrated IMERG precipitation and GLEAM potential evapotranspiration products for drought monitoring over mainland China. *Atmospheric Research*, 247, 105141. https://doi.org/10.1016/j.atmosres.2020.105141.

Kalnay, E., Kanamitsu, M., Kistler, R., Collins, W., Deaven, D., Gandin, L., Iredell, M., Saha, S., White, G., Woollen, J., Zhu, Y., Leetmaa, A., Reynolds, R., Chelliah, M., Ebisuzaki, W., Higgins, W., Janowiak, J., Mo, K. C., Ropelewski, C., . . . Joseph, D. (1996). The NCEP/NCAR 40-year reanalysis project. *Bulletin of the American Meteorological Society*, 77(3), 437–471. https://doi.org/10.1175/1520-0477(1996)077<0437:tnyrp>2.0.co;2.

Khaddor, I., Achab, M., Soumali, M. R., & Alaoui, A. H. (2017). Rainfall-runoff calibration for semi-arid ungauged basins based onthe cumulative observed hyetograph and SCS storm model: Application to the Boukhalef watershed (Tangier, NorthWestern Morocco). *Journal of Materials and Environmental Science*, 8(10), 3795–3808.

Le, H. M., Sutton, J. R., Bui, D. D., Bolten, J. D., & Lakshmi, V. (2018). Comparison and bias correction of TMPA precipitation products over the lower part of red–Thai Binh River basin of Vietnam. *Remote Sensing*, 10(10), 1582.

Marzouk, O. A. (2021). Assessment of global warming in Al Buraimi, sultanate of Oman based on statistical analysis of NASA POWER data over 39 years, and testing the reliability of NASA POWER against meteorological measurements. *Heliyon*, 7(3), e06625.

Motohashi, K., & Motohashi, K. (2015). Changes in the global economic environment. In *Global Business Strategy: Multinational Corporations Venturing into Emerging Markets* (pp. 41–55). Springer.

Prediction of Worldwide Energy Resources. (2022). *POWER data methodology*. https://power.larc.nasa.gov/docs/methodology/

Saber, M., & Yilmaz, K. K. (2018). Evaluation and bias correction of satellite-based rainfall estimates for modelling flash floods over the Mediterranean region: Application to Karpuz River Basin, Turkey. *Water*, 10(5), 657.

Satgé, F., Xavier, A., Pillco Zolá, R., Hussain, Y., Timouk, F., Garnier, J., & Bonnet, M.-P. (2017). Comparative assessments of the latest GPM mission's spatially enhanced satellite rainfall products over the main Bolivian watersheds. *Remote Sensing*, 9(4), 369. https://doi.org/10.3390/rs9040369.

Shah, R., & Mishra, V. (2014). Evaluation of the reanalysis products for the monsoon season droughts in India. *Journal of Hydrometeorology*, 15(4), 1575–1591. https://doi.org/10.1175/JHM-D-13-0103.1.

Singh, J., Knapp, H. V., Arnold, J. G., & Demissie, M. (2005). Hydrological modeling of the Iroquois river watershed using HSPF and SWAT 1. *JAWRA Journal of the American Water Resources Association*, 41(2), 343–360.

Song, X., Kong, F., & Zhu, Z. (2011). Application of Muskingum routing method with variable parameters in ungauged basin. *Water Science and Engineering*, 4(1), 1–12.

Stackhouse, P. W. Jr., Chandler, W. S., Zhang, T., Westberg, D., Barnett, A. J., & Hoell, J. M. (2016). *Surface meteorology and solar energy (SSE) release 6.0 methodology. Version 3.2.0.* Retrieved January 10, 2017, from https://eosweb.larc.nasa.gov/sse/documents/SSE6Methodology.pdf.

Sun, S., Shi, W., Zhou, S., Chai, R., Chen, H., Wang, G., Zhou, Y., & Shen, H. (2020). Capacity of satellite-based and reanalysis precipitation products in detecting long-term trends across Mainland China. *Remote Sensing*, 12(18), 2902. https://doi.org/10.3390/RS12182902.

Tapiador, F. J., Turk, F. J., Petersen, W., Hou, A. Y., García-Ortega, E., Machado, L. A. T., Angelis, C. F., Salio, P., Kidd, C., Huffman, G. J., & de Castro, M. (2012). Global precipitation measurement: Methods, datasets and applications. *Atmospheric Research*, 104–105, 70–97. https://doi.org/10.1016/j.atmosres.2011.10.021.

Tassew, B. G., Belete, M. A., & Miegel, K. (2019). Application of HEC-HMS model for flow simulation in the lake Tana Basin: The case of Gilgel Abay Catchment, upper blue Nile Basin, Ethiopia. *Hydrology*, 6, 21. https://doi.org/10.3390/hydrology6010021.

USDA-NRCS. (1986). *Urban hydrology for small watersheds-technical release 55*. US Department of Agriculture Natural Resources Conservation.

Yu, C., Hu, D., Liu, M., Wang, S., & Di, Y. (2020). Spatio-temporal accuracy evaluation of three high-resolution satellite precipitation products in China area. *Atmospheric Research*, 241, 104952. https://doi.org/10.1016/j.atmosres.2020.104952.